2024 IEEE/RSJ International Conference on Intelligent Robots and Systems (IROS)
October 14-18, 2024. Abu Dhabi, UAE

Multistable Soft Actuator for Physical Human-robot Interaction

Juncai Long, *Student Member, IEEE,* Jituo Li, *Member, IEEE,* Xiaojie Diao, Chengdi Zhou, Guodong Lu, *Member, IEEE,* Yixiong Feng

***Abstract*— Collaboration with robots through physical contact offers a more intuitive, natural, and engaging operational experience, showcasing vast potential in the field of human-robot interaction. However, current physical interaction devices, such as collaborative robots and haptic feedback mechanisms, are limited by their singular modes of motion and feedback, hindering enhancements in interaction experiences. Herein, we present a multistable soft actuator capable of driving multimodal shape changes and passively conforming to user touch. This actuator can memorize and maintains any deformation with zero power consumption. Its structural mechanical properties can be dynamically adjusted to produce rich haptic feedback for the user, including changes in shape, elasticity, stiffness, and even sensations of rupture and weightlessness. Structurally, the mechanism consists of a network of pneumatic bistable units in series and parallel configurations, which can switch states under air pressure or external force, achieving extension, contraction, and omnidirectional bending. The input of air pressure can either impede or assist deformation, altering structural stiffness and resulting in varied loading curves. With its high safety in physical interactions, robust operability, and rich mechanical tactile feedback, the multistable soft actuator promises new design directions for physical human-robot interaction devices.**

***Index Terms* – soft robotics, multistable structure, human-robot interaction, mechanical performance**

I. Introduction

With the advancement of technologies such as metamaterials, artificial intelligence, sensing and control, robots have gradually evolved from simple task performers to autonomous and intelligent companions. Human-robot collaboration is poised to become an important work paradigm in the future [1].

Physical interaction in human-robot collaboration offers unique advantages. Humans can directly communicate with machines through touch and force transmission, while machines perceive information about human actions and force, responding and providing feedback accordingly. This mode of physical interaction fosters a more intuitive, natural, and cohesive human-robot interaction experience, enabling better control and manipulation of machines by humans, and enhancing the machine's ability to understand and respond to human needs.

Research supported in part by the National Natural Science Foundation of China (Grant No. 52275276) and Technology Innovation Project of Yuyao City (Grant No. 2022JH03010006).

Corresponding author: Jituo Li (Email: jituo_li@zju.edu.cn).

Juncai Long, Jituo Li, Xiaojie Diao, Chengdi Zhou, Guodong Lu, and Yixiong Feng are with State Key Laboratory of Fluid Power and Mechatronic Systems, School of Mechanical Engineering, Zhejiang University, Hangzhou 310007, China. They are also with Zhejiang University Robotics Institute. (Email: 12025082@zju.edu.cn; jituo_li@zju.edu.cn; 22225092@zju.edu.cn; 11725072@zju.edu.cn; lugd@zju.edu.cn; fyxtv@zju.edu.cn).

Safety is the foremost consideration in physical interactions. Initially, there was a general inclination to avoid physical contact between robots and humans. The advent of collaborative robots, however, has facilitated safe human-robot interactions [2]. Nonetheless, these collaborative robots rely on torque sensors at the joints and tactile sensors distributed over their surfaces. The significant costs associated with the hardware, coupled with the complexity of the control systems, limit their application space. Moreover, the rigid exteriors of these robots continue to pose a significant challenge to interaction safety.

The metaverse [3], powered by Virtual Reality (VR) and Augmented Reality (AR), presents another avenue for collaboration. It creates virtual environments that realistically simulate the sensory perceptions of a physical world from a first-person perspective. However, the lack of physical peripherals in bare-hand interaction scenarios means tactile feedback is inherently absent. At present, devices designed for tactile feedback often rely on inducing basic tactile sensations on the hand [4], [5], [6], [7], [8] or skin [9], [10] using vibrations or electrical stimulations, providing interfaces [11], [12], [13] or employing linkage mechanisms [14], [15] that deform to restrict movement. This starkly contrasts with the diverse tactile experiences in the physical world, where touch enables the perception of natural objects' shapes, movements, stiffness, and flexibility, including sensing the breakage of fragile items. The simplicity of the current tactile feedback devices in terms of deformation modes and force feedback significantly limits the depth of interaction that can be achieved.

Herein, we design a multistable soft actuator for physical human-robot interaction, elaborating on its mechanism, design principles, materials, and mechanical properties. This soft actuator is capable of actively producing extensions, contractions, and omnidirectional bending to engage with users actively. It can also passively conform upon touch or force transmission by a user, maintaining its deformed state without the need for continuous force input. Furthermore, the actuator's mechanical properties can be dynamically adjusted, altering its structural rigidity and interaction force to enable users to experience a range of tactile sensations.

Figure 1 illustrates our hexagonal multistable actuator, where a pneumatic bistable unit is embedded within each edge. These units can reversibly switch between two stable states when the applied air pressure or external force reaches the loading threshold for state transition. When all six sides deform synchronously, the actuator undergoes uniform extension or contraction, as shown in Figure 1(b). In contrast, asymmetric deformation of the sides results in the actuator exhibiting bending. Notably, the actuator's deformation does not require the maintenance of external force, allowing for the

physical encoding and storage of interaction information under passive conditions. The inherent compliance of the multistable soft actuator and its capacity for passive interaction ensure safe user operation.

During the transition from one stable state to another, multistable structures exhibit both positive and negative stiffness intervals [16], [17]. These intervals can be modulated by air pressure. Similar to interactions in the physical world, when users actively press and touch the multistable actuator, the actuator applies a reactive force, generating real-time tactile feedback. Figure 1(c) and Figure 1(d) demonstrates common scenarios where humans can easily distinguish between objects based on their unique intrinsic property—stiffness. By utilizing stable state transition effects, we simulate the mechanical tactile feedback of pressing and non-rebounding after pressing of a self-locking button, as shown in Figure 1(e). Notably, during paper tearing in Figure 1(f), the sudden loss of positive stiffness evokes a sensation of weightlessness and falling. The multistable actuator mimics the shape, motion, hardness, and flexibility of various objects through deformation and positive stiffness. It can also simulates the sensation of weightlessness during tearing and falling by rapidly switching between positive and negative stiffness.

In conclusion, the multistable soft actuator we have developed facilitates physical interactions between humans and robots through both deformation and force, presenting four innovative aspects:

- A compliant structure with multimodal deformability for safe physical human-robot interaction.
- Adjustable mechanical properties for rich forms of tactile feedback.
- Power-free shape retention for the storage of interactive information.
- Reconfigurable framework for enhancing functionality and expanding applications.

II. Design of the Multistable Soft Robotic Actuator

A. Design principle

Bistable structures subjected to vertical loads exhibit a variety of post-critical behaviors, including snap-through and bifurcation phenomena [18], which find extensive applications across diverse fields such as multimodal grippers [19], [20], [21], morphing structures [22], metamaterials [23], [24], and energy harvesting[25].

Bistable units are characterized by two stable states, allowing for reversible switching between contraction and extension when the driving force exceeds a specific loading threshold. We serially and parallelly combine bistable structures to enrich their deformation behaviors and tailor their mechanical properties. Utilizing the asymmetric deformation of parallel bistable structures, we have engineered hexagonal multistable actuators capable of multidirectional bending deformations. By serially connecting multistable actuators, the types and range of deformation of the structure can be further expanded. This approach enhances the versatility and adaptability of the system, allowing for more complex and extensive applications in various fields.

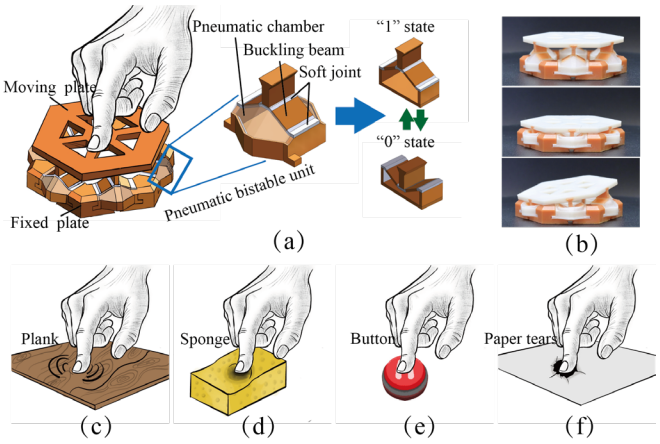

Figure 1. Multistable soft actuator for physical human-robot interaction. (a) Structure of the actuator and its pneumatic bistable counterparts. (b) Deformation behaviors of the physical actuator. (c)-(f) Typical tactile feedback capabilities, exemplified by the stiffness of wood, the compliance of sponges, the activation of self-locking buttons, and the process of paper tearing.

Our pneumatic control strategy preserves the inherent compliance of multistable structures, allowing for active deformation and dynamic adjustment of their mechanical characteristics. This approach has potential applications beyond simulating mechanical touch through force feedback, including the development of soft grippers with adaptable gripping forces and rehabilitation gloves designed to enhance grip strength while providing customizable resistance for strength recovery.

B. Structure design and multimodal deformation

The pneumatic bistable unit (Pneu-bit) comprises a rigid support structure, two buckling beams, three flexible joints, and a sealed chamber, as illustrated in Figure 1(a). The support structure and buckling beams are fabricated from rigid materials, while the membrane of the sealed chamber and the soft joints are made from flexible materials to provide enhanced pliability for repeated stretching and bending. The Pneu-bit incorporates an air hole on its base plate that connects to a pneumatic control system via tubing. This pneumatic system is capable of generating controllable positive and negative pressures. When negative pressure is applied to the sealed chamber, it contracts, inducing a stable state transition of the Pneu-bit from state "1" to state "0". Through deformation of its buckling beams and flexible joints under external force or internal air pressure, the Pneu-bit achieves reversible motion and stable state transitions. This design eliminates the need for additional moving pairs and components, thereby enabling assembly-free integration and manufacturability through 3D printing.

By connecting Pneu-bits in parallel, we have developed a hexagonal multistable soft actuator (HexMSA). Each Pneu-bit can be swiftly connected and replaced through a dovetail joint structure. As illustrated in Figure 1(b), when all Pneu-bits transition from state "1" to state "0" (or from state "0" to state "1"), the HexMSA undergoes a contraction deformation (or extension deformation). When Pneu-bits on opposite sides switch to the opposite state ("0" or "1"), the HexMSA bends towards the side in state "0".

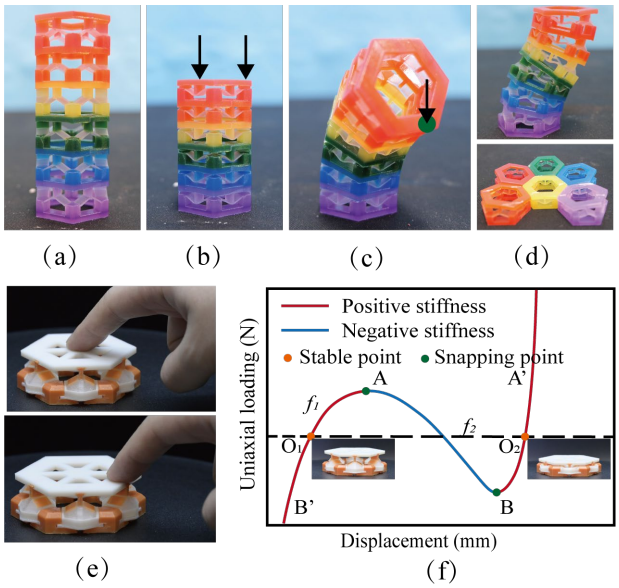

Figure 2. Multimodal deformation and state transition of the hexagonal multistable soft actuator (HexMSA). (a) Six serially connected HexMSAs in the "1" state. Here, the enclosed chambers of HexMSAs are removed for showing the truss structure clearly. (b) The serial HexMSAs compressed. (c) The serial HexMSAs bent. (d) Achieving richer deformation modes through serial and parallel strategy. (e) Interacting by pressing the center or edge of the HexMSA. (f) Mechanical curves during loading.

Further serial connection of HexMSAs allows for the a more diverse range of deformations. As depicted in Figure 2(a) to 2(c), the total displacement of the serially connected body equates to the sum of displacements from each serial unit, and similarly, the bending angle is the aggregate of bending angles from each unit. This configuration enables serial HexMSAs to reach a wider deformation range and to produce a variety of deformation types through deformation combinations, as illustrated in Figure 2(d). In the serially connected body, load sharing among HexMSAs ensures that the body's mechanical behavior is determined by the count and states ("0" and "1") of HexMSAs in series, independent of their spatial configuration. When the serially connected body's load reaches the threshold for a stable state transition, all HexMSAs in the "1" state will sequentially undergo a contraction deformation. The modular design, reconfigurable structure, and the stable states switching features of HexMSA ensure that the mechanical behavior of its serial assemblies is predictable and reprogrammable. This underlines the system's adaptability and precision, enabling customization and reconfiguration of mechanical responses based on specific requirements.

C. *Mechanical properties*

Under uniaxial loading as illustrated in Figure 2(e), HexMSA are capable of reversibly switching between stable states. During the state transition, intervals of positive and negative stiffness are observed. As depicted in Figure 2(f), under displacement-controlled conditions, the HexMSA exhibit an N-shaped force-displacement response curve. The loading process features two phases of positive stiffness, denoted as f_1 (from B' to A) and f_3 (from B to A'), and one phase of negative stiffness, f_2 (from A to B). Between the two phases of positive stiffness, the unit reveals two stable states, labeled "O_1" and "O_0". Initiating from these stable states, two distinct load-displacement paths emerge. A unit in state "1" enters a negative stiffness phase upon reaching peak load F (moving from O_1 through A to B), while a unit in state "0" demonstrates a continuous increase in load (directly to A').

When users physically interact with HexMSAs by pressing, the mechanical process resembles the loading curve under displacement-controlled conditions. By applying varying pressing forces or inflating the HexMSA with different air pressures, HexMSAs undergo distinct deformation stages, producing varied force feedback effects. This results in diverse tactile experiences for the user. The impact of air pressure on the structural stiffness and the force-displacement response curve of the HexMSA is extensively modeled and analyzed in Section III. Intuitively, the presence of positive pressure within the HexMSAs' air chambers impedes contraction deformation (state "1" to "0"), enhancing the effect of positive stiffness phase, whereas negative pressure facilitates contraction, weakening the positive stiffness effect.

III. Mechanical Behavior and Interaction Space

A. *Structural stability and regulation mechanism*

In this study, users primarily interact with multistable soft actuators through pressing actions, so our analysis focus on the mechanical responses to uniaxial compression. To clarify the impact of structural and material parameters, as well as pneumatic control on the stability of pneumatic bistable units, we analyze structural stability based on the assumption of homogeneous deformation, thereby disregarding Euler buckling [26].

In the configuration shown in Figure 3(a), the pneumatic bistable unit's transition between stable states is primarily driven by the deformation of its soft joints and the buckling beams, conceptualized for analysis as a truss system shown in Figure 3(b). The system comprises two beams characterized by an elastic modulus K_1 and length L_r, interconnected via a soft joint at node C_0. The terminal support beam, with a length of L_j and an elastic modulus K_3, is the soft joint attached to the structure's fixed base. An external force F is exerted at C_0, targeting the Z axis in the global coordinate system C_1XYZ, leading to a vertical displacement ω of C_0 and a consequent compression of the buckling beam L_r to a new length l_r.

When the force F is applied at point C_0, the conservative system's total potential energy, denoted as Π, is the sum of two components: the elastic potential energy E and the potential energy attributed to the external force W.

$$\Pi = E + W = K_1(L_r - l_r)^2 - F\omega \tag{1}$$

where,

$$l_r = \sqrt{B^2 + (H - \omega)^2} \tag{2}$$

$$L_r = \sqrt{B^2 + H^2} \tag{3}$$

Here, B and H denote the half-width and the height of the truss system, respectively. Consequently, the relationship between force and displacement within the truss system can be described as:

$$F = \frac{\partial E}{\partial \omega} = 2K_1(H-\omega)\left(\sqrt{\frac{(B^2+H^2)}{B^2+(H-\omega)^2}}-1\right) \quad (4)$$

Depicted by Figure 4(a), ideally, the force-displacement curve ($K_2/K_1 = 0$) exhibits symmetry around the zero-force point ($\omega/H = 1.0$), reached when both springs achieve a horizontal orientation. Nevertheless, the introduction of positive pressure air into the pneumatic bistable unit leads to a modification of its stable state. The modification can be equivalently modeled by the vertical integration of an additional elastic spring, with stiffness K_2, at point C_0, as depicted in Figure 3(c). Consequently, the elastic potential energy of the system can be expressed as

$$E = K_1(L_r - l_r)^2 + \frac{1}{2}K_2\omega^2 \quad (5)$$

Thus, the relationship between force and displacement is

$$F = 2K_1(H-\omega)\left(\sqrt{\frac{(B^2+H^2)}{B^2+(H-\omega)^2}}-1\right) + K_2\omega \quad (6)$$

As depicted in Figure 4(a), with $K_2/K_1 > 0$, the system's symmetry is disrupted by the spring K_2, leading to a displacement shift of the zero-force point to a higher position. The curve rises as K_2/K_1 increases, and when it surpasses a specific value, it no longer intersects with the zero-force horizontal line (F = 0), thereby converting the bistable system into a monostable one. Further increments in K_2/K_1 alter the force-displacement curve of the monostable system from a non-monotonic function, showcasing positive to negative to positive stiffness, to a monotonic function characterized by solely positive stiffness. Thus, by gradually increasing the input air pressure P into the pneumatic bistable unit, it's possible to modulate the stability, adjusting the mechanical curve, and amplifying the force peak of the truss system. Ultimately, the bistable system undergoes a transition to a monostable structure that exhibits mechanical response like elastic materials.

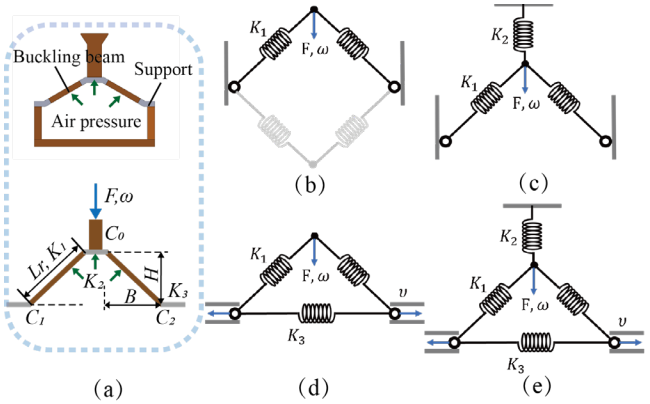

Figure 3. The equivalent truss system of a Pneu-bit. (a) Parameters of the truss system. (b) The truss model without external excitation (K_2=0) under fixed boundary conditions ($K_3 \to \infty$). (c) The truss model with external excitation (K_2) under fixed boundary conditions ($K_3 \to \infty$). (d) The truss model without external excitation (K_2=0) under non-fixed boundary conditions (K_3). (e) The truss model with external excitation (K_2) under non-fixed boundary conditions (K_3).

The terminal constraints of bistable unit are achieved through the utilization of soft joints, which prevent the establishment of entirely fixed boundary conditions. Consequently, to depict the structural stability associated to lateral extension and contraction, it becomes imperative to utilize horizontal linear springs with a modulus of elasticity denoted by K_3, as illustrated in Figures 3(d) and 3(e). When the lateral displacement on one side is given as v, the system's elastic potential energy, as outlined in Figure 3(d), is calculated as

$$E = K_1(L_r - l_r)^2 + 2K_3v^2 \quad (7)$$

where,

$$l_r = \sqrt{(B+v)^2 + (H-\omega)^2} \quad (8)$$

Similarly, the elastic potential energy of the system illustrated in Figure 3(e) is

$$E = K_1(L_r - l_r)^2 + \frac{1}{2}K_2\omega^2 + 2K_3v^2 \quad (9)$$

The relationship between force and displacement of the system can be solved by the following equation

$$\begin{pmatrix} \frac{\partial E}{\partial \omega} \\ \frac{\partial E}{\partial v} \end{pmatrix} = \begin{pmatrix} F \\ 0 \end{pmatrix} \quad (10)$$

As shown in Figure 4(c) and 4(d), when $K_2/K_1 = 0$ (or $K_2/K_1 = 0.1$), the peak values of the force-displacement curve for the symmetric (or asymmetrical) bistable system increase with the increment of K_3/K_1, albeit the magnitude of increase diminishes progressively. The expression $K_3/K_1 \to \infty$ represents the condition of completely fixed terminal constraint.

Similar to the ratio of K_3/K_1, the geometric parameter H/B can also enhance the loading threshold for steady-state transition. When $K_2/K_1 = 0$, the peak values of the force-displacement curves for symmetrical bistable systems increase progressively with H/B. For cases where $K_2/K_1 > 0$ and H/B is relatively small, the truss structure exhibits a monotonic increase in the force-displacement curve. At this case as shown in Figure 4(d), the system is a monostable system, with the curve remaining above $F = 0$ ($F > 0$). As H/B increases, the curve evolves from a monotonic function with positive incremental stiffness to a non-monotonic function exhibiting sequences of positive-negative-positive incremental stiffness. With further increases in H/B, negative forces ($F < 0$) emerge, transitioning the system from a monostable to an asymmetrical bistable system.

The transition mechanisms of bistable and multistable systems are determined by material properties and geometric parameters of the supporting beams and the buckling beams. Once the structure of a pneumatic bistable unit is established, its mechanical properties can be dynamically adjusted through air pressure.

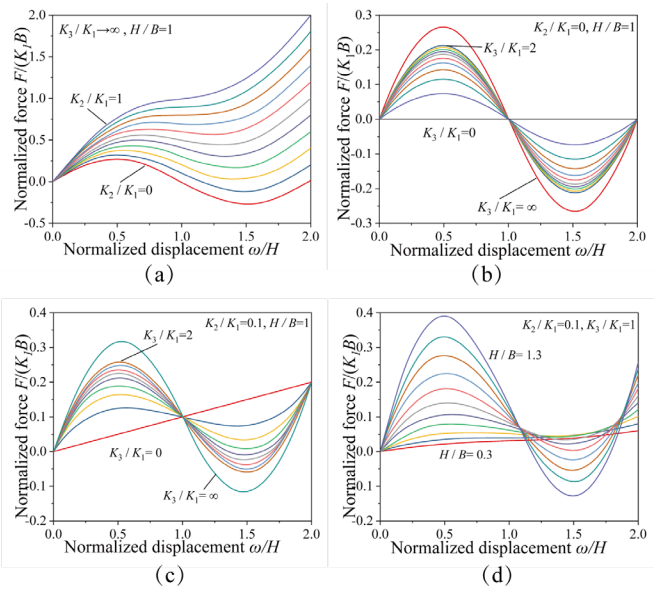

Figure 4. Stability of the truss system. (a) Under fixed boundary constraints (K_3=0), the impact of external excitation (K_2) on stability. (b) With no external excitation (K_2=0), the influence of boundary constraints (K_3) on stability. (c) With external excitation present (K_2=0.1K_1), the effect of boundary constraints (K_3) on stability. (d) With external excitation (K_2=0.1K_1), the impact of structural parameters (H/B) on stability.

B. *Design of interaction space*

The inherent compliance, multistable snapping mechanisms, multimodal deformation capabilities, and tunable mechanical properties of HexMSA offer unique advantages in physical human-robot interactions.

Shape, motion, and force constitute the three fundamental elements of physical interaction. The interaction of shape and motion is bidirectional. Users can freely manipulate the shape of HexMSAs and perceive the actuated deformations through touch. Deformations and motions are, in essence, outcomes of force interactions. Pneumatic bistable unit drives deformation in HexMSAs, resulting in the output of force; similarly, users input force into HexMSAs through touch, causing adaptive shaping. Each HexMSA is designed with a preset force threshold that resists applied pressure up to a certain limit, beyond which deformation occurs. The preset force, determined by material properties, structural parameters, and air pressure control, act as the threshold for stable state transition. The combination of shape, motion, and force enables the construction of abundant haptic experiences.

The compliance response behaves similarly to compressing a spring or elastic material, where the feedback force progressively increases as the user presses deeper. As illustrated by the load curve in Figure 4(a), the bistable curve of the pneumatic bistable unit gradually transitions to a monostable curve with positive incremental stiffness as the internal pressure continuously increases. In this manner, it's possible to approximate the tactile sensation of various elastomers.

Humans are capable of qualitatively determining the hardness of a material through touch, but they fall short in accurately evaluating its precise stiffness. This shortfall arises from the hands' inability to generate the sufficient force to induce perceptible deformations. In our design, when all connected HexMSAs transition from a state of "1" to "0", there is a minor deformation upon application of pressure, effectively showcasing the load-bearing features of rigid materials.

Layer snapping response is a distinctive tactile effect. It occurs when the surface shape deforms to a predefined elevation as force is exerted by a user on the interactive layer. Different layers may have varied force thresholds, facilitating the communication of characteristics (such as hardness and softness) between layers. The layer snapping effect is enabled by assigning different loading thresholds to the HexMSAs in series. When the load on the serial HexMSAs attains the designated steady-state switching threshold, a sequential snap-through event occurs in all HexMSAs that are in the "1" state.

Weightlessness, experienced during events such as breaking or falling, as illustrated in Figure 1(f), often elicits a profound sensory impact on the human body. The mechanical response observed during the stable states switching of bistable structures, transitioning from positive to negative stiffness, exhibits a close alignment with the mechanical responses witnessed in breaking and tearing phenomena. As illustrated in Figure 4(b) and 4(d), the greater the value of K_3 and H/B and the larger the difference between positive and negative stiffness, makes the sensation of weightlessness more pronounced.

IV. Experimental Results

To verify the inherent compliance, multistable mechanism, multimodal deformation capability, and tunable mechanical properties of the HexMSA, we fabricated a physical prototype of the HexMSA and conducted performance validation tests.

A. *Control and fabrication*

A pneumatic control system is utilized to control air pressure and vacuum degree, interfacing with multistable soft actuator through flexible silicone tubes. As demonstrated in Figure 5(a), the system adjusts the pressure of the airflow from the pump using a pressure regulating valve. This setup allows for the conversion of positive pressure into vacuum pressure via a vacuum generator, with the current pressure level being displayed on a pressure gauge. Control over the airflow circuit is achieved through the deployment of multiple three-way solenoid valves.

To fabricate this multimaterial design, we utilized a multimaterial 3D printer (J300, Sailner 3D Inc., China), capable of printing structures with diverse mechanical properties by mixing elastic and rigid materials in different proportions. The substrates RGD110T, the soft FLX910T (30A), and the ultra-soft FLX920W (10A) exhibit varying Shore hardness values (unit: A). Following printing, as illustrated in Figure 5(b), the support material from the prints was first removed, then the prints were soaked and ultrasonically cleaned in a 5% NaOH solution to eliminate any residual support material. Finally, the prints were subjected to a secondary ultraviolet curing process to enhance the structural strength. The Figure 5(c) displays the assembled multistable soft actuator.

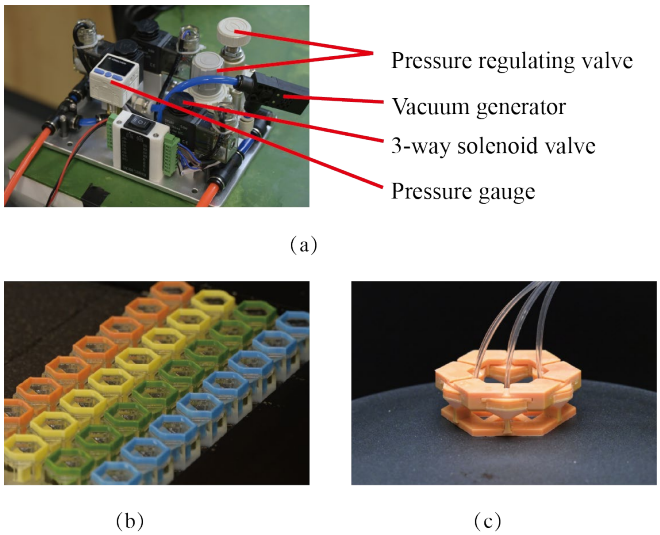

Figure 5. Control and fabrication of HexMSA. (a) Pneumatic control system. (b) 3D printed pneumatic bistable units. (c) Assembled multistable soft actuator.

B. *Multimodal deformation*

By serially connecting HexMSAs, a larger deformation range and a wider variety of deformation types can be achieved. Consequently, HexMSAs offer an expanded working space, affording users greater freedom in manipulation.

Figure 6 illustrates a configuration involving three HexMSAs connected in sequence. The soft joints of the HexMSAs, colored orange, yellow, and green, utilize materials of differing stiffness. The orange HexMSA's material is the most flexible and the green is the most rigid. Each HexMSA has a length of 20mm, with a maximum displacement close to 6mm, and achieves a bending angle of approximately 10°.

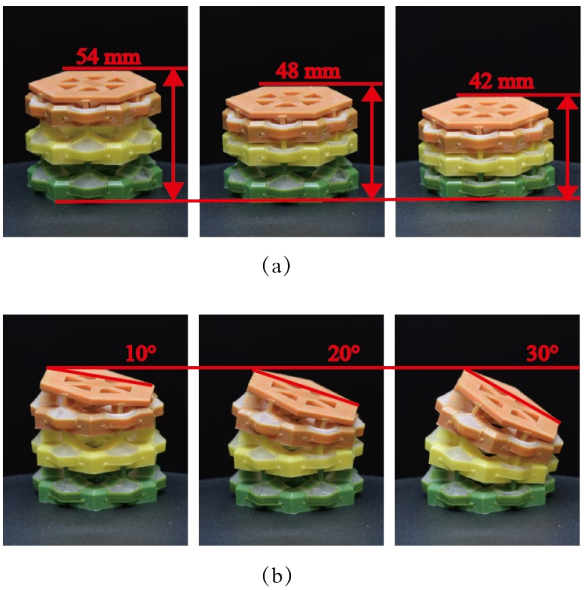

Figure 6. Multimodal deformation of HexMSAs. (a) Layered contraction deformation. (b) Layered bending deformation.

As we apply pressure to the midpoint of connected HexMSAs with our hands, the escalation of force first leads to the contraction deformation of the orange HexMSA. Increasing the pressure further results in a sequential deformation of the orange, yellow, and green HexMSAs, achieving a collective displacement of 18mm, which is the exact sum of the individual displacements of the three HexMSAs. Likewise, the total bending angle of the interconnected HexMSAs is the sum of the bending angles of the individual HexMSAs. Moreover, more diverse deformation is attainable by integrating various deformation modes from each actuator, such as combinations of bending in different directions and contracting deformations. Theoretically, the HexMSAs can undergo infinite extension to accommodate diverse needs.

C. *Adjustable mechanical behavior*

HexMSA's mechanical responses are affected by various factors, such as the choice of material, structural design, and external stimulation. We undertake an evaluation of the mechanical properties of HexMSAs that have been constructed using diverse materials and stimulated with different levels of air pressure. A tensile testing machine is used, as illustrated in Figure 7(a). The measurement range is 0-50 N, the resolution of force is 0.001 N, and the resolution of displacement is 0.01 mm. The tensile tests were performed using a displacement-controlled loading mode at a constant test speed of 40 mm/min.

Initially, we performed a calibration of the three materials utilized in the fabrication of the HexMSAs, with the fitted curves illustrated in Figure 7(b). The soft joints in the orange HexMSA were made exclusively from FLX910 material, whose hardness is around 30A. Meanwhile, the yellow and green HexMSAs' soft joints incorporated the stiffer RGD110 material, resulting in hardness levels of 50A and 65A, respectively. When loading each of the three actuators separately, the loading curves obtained are displayed in Figure 7(c). It was observed that an increase in the hardness of the soft joints leads to a greater loading threshold for the actuators they form part of. Nonetheless, this increase in hardness does not impact the structural stability or change the monotonicity of the loading curves, which is consistent with the results in Figure 4(b) and 4(c).

The mechanical characteristics of the orange HexMSA are dynamically regulated by modifying the pressure of its internal gas. As indicated in Figure 7(d), with no gas input, the actuator presents an asymmetric bistable structure under the influence of uniaxial force. The process of shifting from state "1" to state "0" demands a higher loading threshold than the transition from state "0" to state "1". This disparity arises from the actuator's fabrication in state "1" via 3D printing. Soft joints store elastic energy during the transition from state "1" to state "0", resulting in a tendency for elastic resilience. Introducing higher positive pressure increases the loading threshold and concurrently transforms the bistable system into a monostable system. On the other hand, negative pressure serves to reduce the loading threshold. The results are consistent with the conclusion presented in Section III.A. The mechanical performance of the HexMSA is substantiated to some degree through experimental testing.

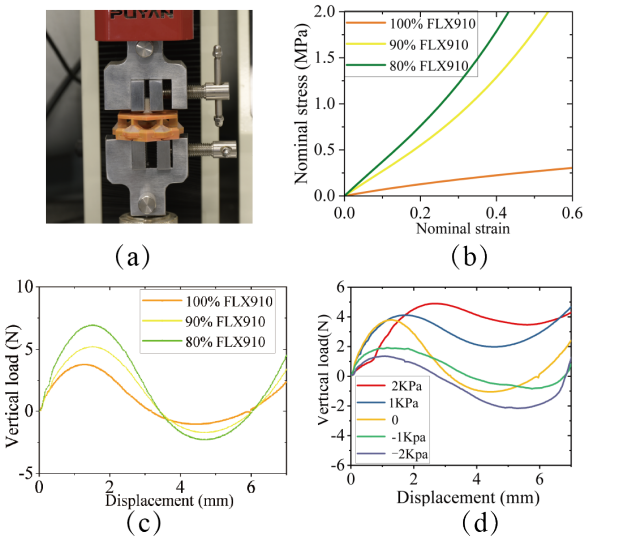

Figure 7. Mechanical behaviors of HexMSAs. (a) Uniaxial loading expriments. (b) Mechanical properties of materials used in manufacturing. (c) Uniaxial vertical loading curves of HexMSAs manufactured from different materials. (d) Uniaxial vertical loading curves of HexMSAs when different air pressures are inputted.

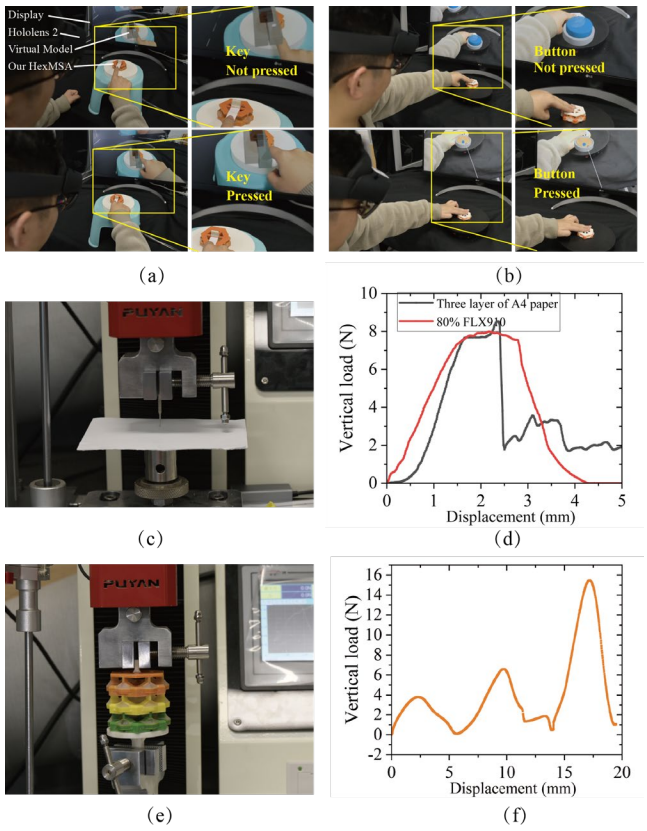

Figure 8. A combination of physical and virtual human-robot interaction. (a) Pressing resettable key. (b) Pressing self-locking button. (c) Puncturing three layers of A4 paper. (d) Curves of puncturing A4 paper and pressing the yellow HexMSA. (e) Uniaxial loading of serially connected HexMSAs. (f) Curves of loading serial HexMSAs.

D. A combination of physical and virtual interaction

To assess the tactile experiences offered by the HexMSA in interactive contexts, we combined the HexMSA prototype with the mixed reality device HoloLens 2 (Microsoft Corporation, USA). The goal was to validate the range and effects of force feedback capabilities provided by HexMSA. The tests includes a resettable key, a self-locking button, a sensation of weightlessness, and layer snapping, as depicted in Figures 1(c)-(f) and elaborated upon in Section III.B. Furthermore, we evaluated the contribution of these tactile sensations, in conjunction with the HoloLens 2, towards augmenting users' immersive experiences.

As illustrated in Figures 8(a) and 8(b), we constructed resettable piano keys and self-locking button within a virtual environment and deployed them for interaction with the HoloLens 2. During interaction with the virtual keys and buttons, the HoloLens 2 provides feedback in the form of sound and visual deformation. Users can capture interaction cues through auditory and visual means. Our HexMSA serves as a tactile feedback device, visually aligning with the virtual model to provide additional mechanical tactile feedback. The virtual piano keys can actively reset upon depression, whereas the self-locking buttons do not reset after being pressed, representing typical monostable and bistable structures, respectively. To simulate the tactile sensation of a monostable piano key more accurately, we adhered white keys to one side of the HexMSA and switched it from a bistable to a monostable system by applying appropriate positive pressure to the corresponding Pneu-bit. Upon depression, both the virtual key model and the physical key deform simultaneously, and both reset when the pressure is released. Similarly, we utilized the bistable characteristic of HexMSA to simulate the self-locking mechanism of the button.

The sensations of weightlessness and layer snapping are unique tactile feedback forms that HexMSA can provided. To verify the effectiveness of the weightlessness sensation provided by HexMSA, we equipped a tensile testing machine with a 0.5mm diameter needle, piercing through three sheets of A4 paper freely placed on a support structure with a 1.2mm diameter hole. Through uniaxial loading, we measured the weightlessness force curve caused by the piercing, as shown in Figure 8(d). There is a high degree of correspondence between this curve and the initial segment of the loading curve for the green HexMSA displayed in Figures 7(b) and 7(c), indicating that HexMSA can accurately and realistically simulates the weightlessness effect. Furthermore, by serially connecting three HexMSAs with different loading thresholds, we achieved the tactile feedback form of layer snapping. A key benefit of HexMSA is its capability to provide varied tactile feedback forms without the reliance on extra structural components.

By integrating the tactile feedback of HexMSA with the HoloLens 2, we provide users with authentic and responsive tactile sensations that are synchronized with the visual and auditory stimuli of the mixed reality (MR) environment, thereby facilitating a more immersive interactive experience in MR scenarios.

V. Conclusion

In this paper, we introduce a multistable soft actuator capable of facilitating physical human-robot interactions. This soft mechanical system offers numerous advantages, including multimodal deformation, adjustable stiffness, zero-power shape retention, rapid response, and abundant extension ability. Its unique properties can potentially find broad applications in fields such as robotic gripping, human-machine interaction, medical applications, and drones, addressing long-standing challenges. For instance, rehabilitation robots for assistive gripping and impedance training, soft grippers with controllable gripping force and stiffness, and load-carrying platforms with conforming and energy buffering capabilities can greatly benefit from this technology. The fully 3D printed structure allows for customization in shape, size, and weight to meet specific demands. The potential of its characteristics, such as body compliance, multistable transition mechanisms, multimodal deformation capabilities, and tunable mechanical properties, remains vast for exploration, offering numerous possibilities for enhancing system performance across various applications.

Acknowledgment

This work was supported in part by National Natural Science Foundation of China 52275276 and Technology Innovation Project of Yuyao City under Grant 2022JH03010006.

References

[1] G. Charalambous, S. Fletcher, and P. Webb, "Identifying the key organisational human factors for introducing human-robot collaboration in industry: an exploratory study," *Int J Adv Manuf Technol*, vol. 81, no. 9–12, pp. 2143–2155, Dec. 2015, doi: 10.1007/s00170-015-7335-4.

[2] A. Hentout, M. Aouache, A. Maoudj, and I. Akli, "Human–robot interaction in industrial collaborative robotics: a literature review of the decade 2008–2017," *Advanced Robotics*, vol. 33, no. 15–16, pp. 764–799, Aug. 2019, doi: 10.1080/01691864.2019.1636714.

[3] M. Sparkes, "What is a metaverse," *New Scientist*, vol. 251, no. 3348, p. 18, Aug. 2021, doi: 10.1016/S0262-4079(21)01450-0.

[4] K. R. Pyun, J. A. Rogers, and S. H. Ko, "Materials and devices for immersive virtual reality," *Nat Rev Mater*, vol. 7, no. 11, Art. no. 11, Nov. 2022, doi: 10.1038/s41578-022-00501-5.

[5] Y. H. Jung, J.-H. Kim, and J. A. Rogers, "Skin-Integrated Vibrohaptic Interfaces for Virtual and Augmented Reality," *Advanced Functional Materials*, vol. 31, no. 39, p. 2008805, 2021, doi: 10.1002/adfm.202008805.

[6] Z. Sun, M. Zhu, X. Shan, and C. Lee, "Augmented tactile-perception and haptic-feedback rings as human-machine interfaces aiming for immersive interactions," *Nat Commun*, vol. 13, no. 1, p. 5224, Sep. 2022, doi: 10.1038/s41467-022-32745-8.

[7] M. Zhu *et al.*, "Haptic-feedback smart glove as a creative human-machine interface (HMI) for virtual/augmented reality applications," *Science Advances*, vol. 6, no. 19, p. eaaz8693, May 2020, doi: 10.1126/sciadv.aaz8693.

[8] Y. Liu *et al.*, "Electronic skin as wireless human-machine interfaces for robotic VR," *Science Advances*, vol. 8, no. 2, p. eabl6700, Jan. 2022, doi: 10.1126/sciadv.abl6700.

[9] K. Yao *et al.*, "Encoding of tactile information in hand via skin-integrated wireless haptic interface," *Nat Mach Intell*, vol. 4, no. 10, Art. no. 10, Oct. 2022, doi: 10.1038/s42256-022-00543-y.

[10] E. Leroy, R. Hinchet, and H. Shea, "Multimode Hydraulically Amplified Electrostatic Actuators for Wearable Haptics," *Advanced Materials*, vol. 32, no. 36, p. 2002564, 2020, doi: 10.1002/adma.202002564.

[11] K. Nakagaki, D. Fitzgerald, Z. (John) Ma, L. Vink, D. Levine, and H. Ishii, "inFORCE: Bi-directional `Force' Shape Display for Haptic Interaction," in *Proceedings of the Thirteenth International Conference on Tangible, Embedded, and Embodied Interaction*, Tempe Arizona USA: ACM, Mar. 2019, pp. 615–623. doi: 10.1145/3294109.3295621.

[12] S. Follmer, D. Leithinger, A. Olwal, A. Hogge, and H. Ishii, "inFORM: dynamic physical affordances and constraints through shape and object actuation," in *Proceedings of the 26th annual ACM symposium on User interface software and technology*, St. Andrews Scotland, United Kingdom: ACM, Oct. 2013, pp. 417–426. doi: 10.1145/2501988.2502032.

[13] B. K. Johnson *et al.*, "A multifunctional soft robotic shape display with high-speed actuation, sensing, and control," *Nat Commun*, vol. 14, no. 1, p. 4516, Jul. 2023, doi: 10.1038/s41467-023-39842-2.

[14] C. Pacchierotti, S. Sinclair, M. Solazzi, A. Frisoli, V. Hayward, and D. Prattichizzo, "Wearable Haptic Systems for the Fingertip and the Hand: Taxonomy, Review, and Perspectives," *IEEE Transactions on Haptics*, vol. 10, no. 4, pp. 580–600, Oct. 2017, doi: 10.1109/TOH.2017.2689006.

[15] Q. Xiong *et al.*, "So-EAGlove: VR Haptic Glove Rendering Softness Sensation With Force-Tunable Electrostatic Adhesive Brakes," *IEEE Transactions on Robotics*, vol. 38, no. 6, pp. 3450–3462, Dec. 2022, doi: 10.1109/TRO.2022.3172498.

[16] A. Rafsanjani, A. Akbarzadeh, and D. Pasini, "Snapping Mechanical Metamaterials under Tension," *Adv. Mater.*, vol. 27, no. 39, pp. 5931–5935, Oct. 2015, doi: 10.1002/adma.201502809.

[17] F. O. Falope, M. Pelliciari, L. Lanzoni, and A. M. Tarantino, "Snap-through and Eulerian buckling of the bi-stable von Mises truss in nonlinear elasticity: A theoretical, numerical and experimental investigation," *International Journal of Non-Linear Mechanics*, vol. 134, p. 103739, Sep. 2021, doi: 10.1016/j.ijnonlinmec.2021.103739.

[18] R. V. Mises, "Über die Stabilitätsprobleme der Elastizitätstheorie," *Z. angew. Math. Mech.*, vol. 3, no. 6, pp. 406–422, 1923, doi: 10.1002/zamm.19230030602.

[19] Y. Jiang *et al.*, "Reprogrammable Bistable Actuators for Multimodal, Fast, and Ultrasensitive Grasping," *IEEE/ASME Trans. Mechatron.*, pp. 1–11, 2023, doi: 10.1109/TMECH.2023.3318976.

[20] Y. Zhang, W. Zhang, P. Gao, X. Zhong, and W. Pu, "Finger-palm synergistic soft gripper for dynamic capture via energy harvesting and dissipation," *Nat Commun*, vol. 13, no. 1, p. 7700, Dec. 2022, doi: 10.1038/s41467-022-35479-9.

[21] H. Hsiao, J. Sun, H. Zhang, and J. Zhao, "A Mechanically Intelligent and Passive Gripper for Aerial Perching and Grasping," *IEEE/ASME Transactions on Mechatronics*, vol. 27, no. 6, pp. 5243–5253, Dec. 2022, doi: 10.1109/TMECH.2022.3175649.

[22] L. Jiang *et al.*, "Electroactive Soft Bistable Actuator With Adjustable Energy Barrier and Stiffness," *IEEE Trans. Robot.*, vol. 40, pp. 472–482, 2024, doi: 10.1109/TRO.2023.3331065.

[23] F. Pan, Y. Li, Z. Li, J. Yang, B. Liu, and Y. Chen, "3D Pixel Mechanical Metamaterials," *Adv. Mater.*, vol. 31, no. 25, p. 1900548, Jun. 2019, doi: 10.1002/adma.201900548.

[24] X. Lin *et al.*, "A Stair-Building Strategy for Tailoring Mechanical Behavior of Re-Customizable Metamaterials," *Adv. Funct. Mater.*, vol. 31, no. 37, p. 2101808, Sep. 2021, doi: 10.1002/adfm.202101808.

[25] S. Shan *et al.*, "Multistable Architected Materials for Trapping Elastic Strain Energy," *Adv. Mater.*, vol. 27, no. 29, pp. 4296–4301, Aug. 2015, doi: 10.1002/adma.201501708.

[26] L. Kwasniewski, "Complete equilibrium paths for Mises trusses," *International Journal of Non-Linear Mechanics*, vol. 44, no. 1, pp. 19–26, Jan. 2009, doi: 10.1016/j.ijnonlinmec.2008.08.011.

[27] B. Haghpanah, L. Salari-Sharif, P. Pourrajab, J. Hopkins, and L. Valdevit, "Multistable Shape-Reconfigurable Architected Materials," *Adv. Mater.*, vol. 28, no. 36, pp. 7915–7920, Sep. 2016, doi: 10.1002/adma.201601650.

[28] "Multi-stable mechanical metamaterials by elastic buckling instability | SpringerLink." Accessed: Apr. 21, 2023. [Online]. Available: https://link.springer.com/article/10.1007/s10853-018-3065-y